

SCIENTIFIC REPORTS



OPEN

Matching DMFT calculations with photoemission spectra of heavy fermion insulators: universal properties of the near-gap spectra of SmB_6

Chul-Hee Min¹, F. Goth², P. Lutz¹, H. Bentmann¹, B. Y. Kang³, B. K. Cho³, J. Werner², K.-S. Chen², F. Assaad² & F. Reinert¹

Paramagnetic heavy fermion insulators consist of fully occupied quasiparticle bands inherent to Fermi liquid theory. The gap emergence below a characteristic temperature is the ultimate sign of coherence for a many-body system, which in addition can induce a non-trivial band topology. Here, we demonstrate a simple and efficient method to compare a model study and an experimental result for heavy fermion insulators. The temperature dependence of the gap formation in both local moment and mixed valence regimes is captured within the dynamical mean field (DMFT) approximation to the periodic Anderson model (PAM). Using the topological coherence temperature as the scaling factor and choosing the input parameter set within the mixed valence regime, we can unambiguously link the theoretical energy scales to the experimental ones. As a particularly important result, we find improved consistency between the scaled DMFT density of states and the photoemission near-gap spectra of samarium hexaboride (SmB_6).

The interplay of topology and correlation effects has led to generalizations of the concept of topological insulators^{1,2}, namely to symmetry protected topological surface states (TSS)³. Topological Kondo insulators (TKI)^{4,5} are an example of a time reversal symmetry protected TSS. Here, correlation effects are dominant in the formation of the low-energy quasiparticle excitations, but the ground state itself is believed to be adiabatically connected to a Fermi liquid. In this sense, one can construct a link to a non-interacting fermion system (with heavy mass), and take over our understanding of the \mathbb{Z}_2 classification⁶ to this class of correlated materials^{7–11}. A well-known candidate for the TKI is the compound samarium hexaboride (SmB_6). It is a paramagnetic bulk insulator^{12,13} with a smooth gap opening consisting of $4f$ and $5d$ characters^{14–16}.

The microscopic picture of this particular coherent state has been qualitatively captured with various mean-field approximations to the periodic Anderson model (PAM)^{4,9,14,17–34}. However, a quantitative comparison between theoretical and experimental density of states (DOS) is hampered by the complexity of the actual material and by the experimental processes, *e.g.* surface reconstructions, multiplet structure, line broadening, information depth, etc^{35–37}. Moreover, such quantitative analyses require to identify the validity range of the theoretical results applicable to the experimental data. Hence, it is in general necessary to find a proper energy conversion between theoretical and experimental energies.

The aim of this paper is to present a new perspective on the comparison of theoretical and experimental DOS of heavy fermion (HF) insulators. In particular, we focus on the dynamical emergence of the hybridization gap of topological HF insulators in units of the coherence temperature T_{coh} . This scaling provides an effective way to convert the theoretical to the experimental energy scales. Such scaling approaches have been mainly applied

¹Experimentelle Physik VII and Röntgen Research Center for Complex Materials (RCCM), Universität Würzburg, 97074, Würzburg, Germany. ²Institut für Theoretische Physik und Astrophysik, Universität Würzburg, 97074, Würzburg, Germany. ³School of Materials Science and Engineering, Gwangju Institute of Science and Technology (GIST), Gwangju, 61005, Korea. Correspondence and requests for materials should be addressed to C.-H.M. (email: cmin@physik.uni-wuerzburg.de)

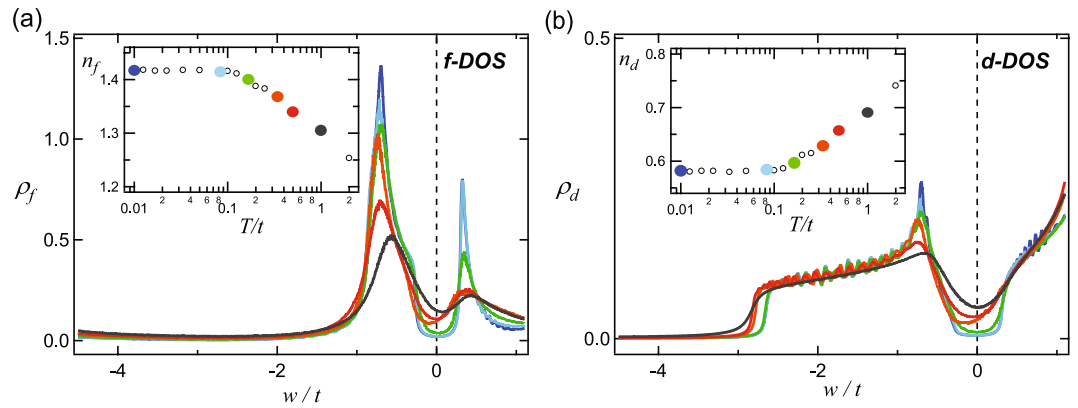


Figure 1. As an example of the DMFT results, temperature (T) dependence for density of f and d states, for the mixed valence regime ($U/t = 5$) is shown in (a) and (b), respectively. The coherence temperature for this regime is $T_N/t = 0.2125$, which is evaluated from index N_2 . The energy is normalized to the hopping parameter t . In the same colors used for density of states (DOS) lines, the corresponding occupation numbers for f and d states are shown as a function of T/t in the insets. The gap, whose character mainly originates from f states at high T , becomes clearer and deeper with decreasing T . Note that at $T \leq T_N$ the spectral weights inside the gap, and the occupation numbers of f and d states start to saturate (insets).

to transport properties of metallic Ce- and Yb-based HF systems^{38,39}. For these metallic cases, there is a certain freedom in defining the quantitative T_{coh} depending on the respective physical properties^{40–42}. This is due to the nature of the crossover in PAM (See also the Sec. I of the Supplementary Information). However, this definition is less ambiguous for the insulating phase. The reason is that most physical properties will drastically change with the gap opening. Thus, T_{coh} can be chosen to mark the temperature at which the gap opens, and can therewith be connected to the topological phase by monitoring the emergence of the TSS^{24,25,28}.

Since the emergent topological band structure is nothing else but evidence for coherence, we can use the net polarization of the TSS to define T_{coh} in the model calculations⁴³. One can define a pseudo-spin Hall conductivity that takes the value of unity at zero temperature in the insulating state, thereby defining a topological index N_2 ^{24,25}. The topological coherence temperature T_N corresponds to the T scale at which the index N_2 takes the value of one-half, *i.e.* the pseudo-spin Hall conductivity of the TSS takes half of its zero temperature quantized value. With the definition of T_N , a unifying crossover parameter can be defined to describe both the lattice coherence and the topological phase. We revisit the physical consequences occurring at the T_N values, which are carefully evaluated in the refs^{24,25}, considering the index N_2 with the same input parameters used in this study. In particular, we analyzed the gap evolution and occupation numbers to extract the experimental results.

Our choice for the theoretical approach is the dynamical mean field theory (DMFT)²⁴. Since we take a simple version of the PAM, our results cannot effectively capture every spectral detail of SmB_6 ³³. Nevertheless, a simplified model has the advantages of surveying unique and general properties in the wide ranges of input parameters. In previous studies, the electron correlation U was tuned from the mixed valent regime to the local moment regime, and we identified universal features in the T -dependent N_2 index^{21,24}. Experimentally, we investigated the near-gap region of SmB_6 by photoemission spectroscopy (PES). There are fascinating low- T properties observed in SmB_6 ^{44–57}, which we do not consider in the present study. Note that, as the energy resolution of the PES setup is limited, PES results have not detected all degenerate f bands predicted in first-principle calculations^{7,8,17,27} in the energy range of 20 meV below the chemical potential^{22,58–63}. Instead, we focus on the gap opening of SmB_6 that is observed in the PES experiments and explains various transport properties near 50 K^{22,62}.

We will first show our theoretical results near T_N and place emphasis on the temperature dependence of the orbital dependent occupation numbers. In the following section, we display the scaled DMFT spectra at different U values, and clarify the universal gap features. Adopting the T_N scaling, we will show consistent results on the gap evolution obtained from theory and experiment. In the discussion section, the importance of the scaling with T_N is described and the key parameters are discussed. In the supplementary information, we give a detailed discussion of the crossover temperature in the Anderson model, additional noteworthy points for the comparisons, and illustrate the detailed spectral weight redistribution in the $E(k)$ plot near T_N . Although our simplified model captures the overall T -dependence of the electronic structure, it fails to properly describe material specific aspects, *e.g.* in present case, the slight slope change in Sm valence at 120 K or the slight increase below 20 K⁶⁴ are not realized in our result.

Results

T -dependence of theoretical DOS and occupation numbers. Figure 1 shows the T -dependence of the f and d density of states (DOS) as a function of energy over hopping parameter for the d states (w/t)²⁴. Here, we illustrate the DOS near $T_N/t = 0.2125$ in the mixed valence regime ($U/t = 5$). In the insets, the occupation numbers n_f and n_d of each DOS are depicted as a function of T/t in the colors corresponding DOS lines. Figure 1(a) shows the occupied f -DOS near E_F which is related to the Hubbard band lying near the chemical potential, and Fig. 1(b) mainly shows the occupied d -DOS, which originates from the 2D conduction band. Both f - and d -DOS are only broadened due to the imaginary part of the self-energy. (The wiggling features in

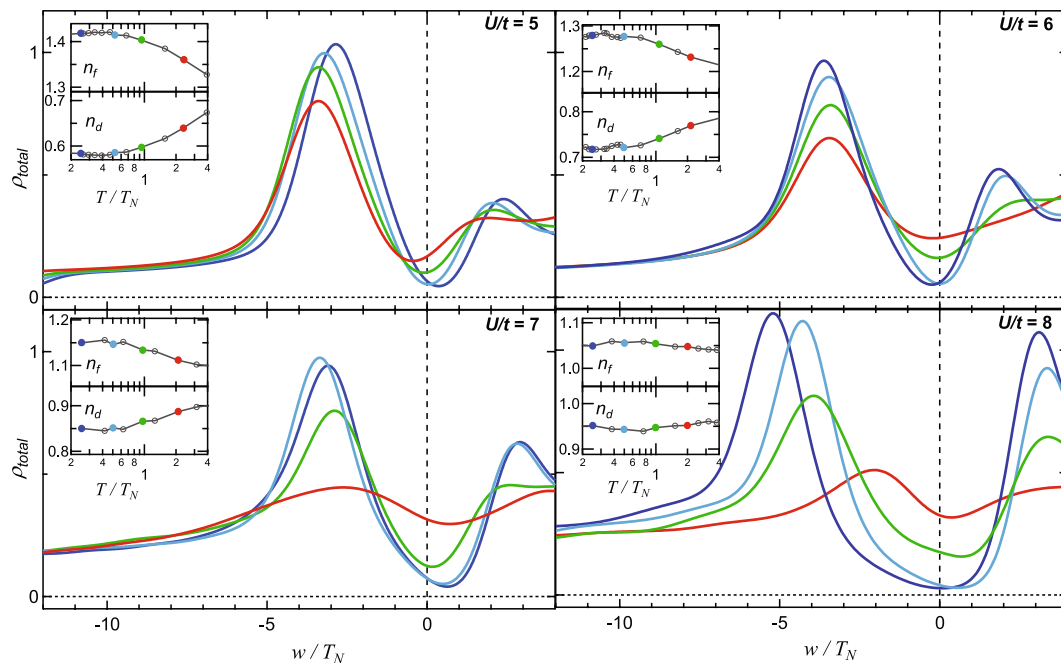


Figure 2. Universal gap evolution studied for $U/t = 5, 6, 7$; and 8 . Total DOS, which are exactly treated as the spectra in Fig. 3(b). The spectral weight in the gap region decreases with decreasing T . The gap region becomes clearer. Insets show the T dependence of the occupation numbers of n_f and n_d for each U values. The occupation numbers vary as a function of T strongly in the mixed valence regime ($U/t = 5$). But, the variation reduces continuously from the mixed valence regime to the local moment regime ($U/t = 8$), which indicates a crossover.

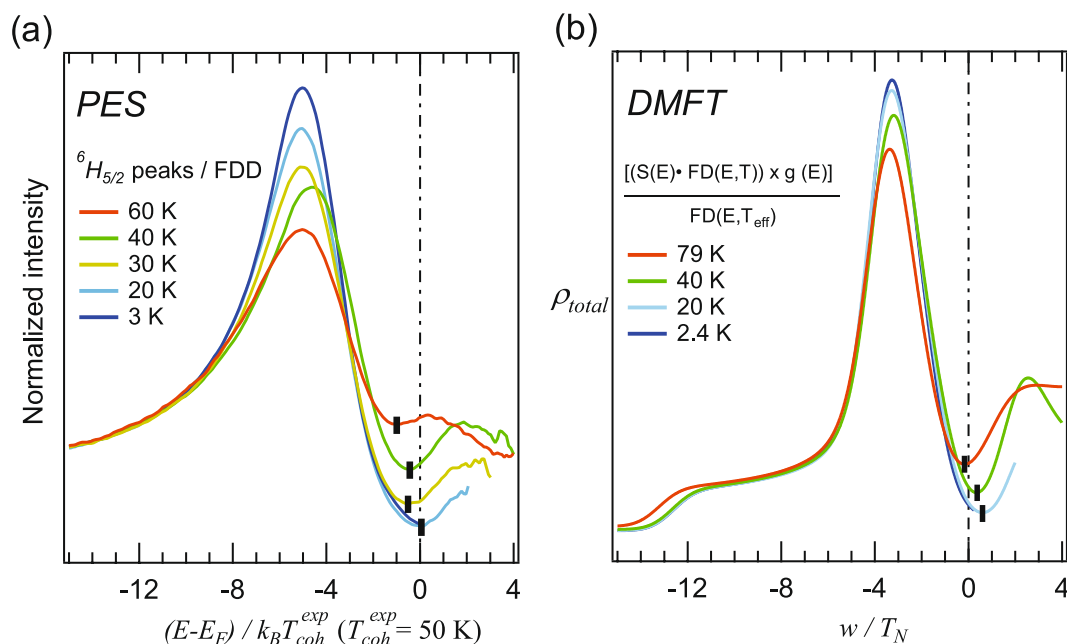


Figure 3. Comparison of the PES spectra of SmB_6 with the theoretical DOS after scaling with the corresponding T_{coh} . (a) The angle-integrated spectra of SmB_6 are divided by the Fermi-Dirac function⁶². The energy axis is reduced by the coherence scale determined from experiments ($T_{\text{coh}}^{\text{exp}} = 50 \text{ K}$). (b) Reconstructed spectra from theoretical calculation, considering Fermi-Dirac distributions and total experimental resolutions (see text), in order to compare with the experiment spectra (a). In unit of the respective coherence energies, the f peaks in (a) and (b) appear at the energy of the same order of magnitude. Moreover, the gap regions show similar T dependence such that the gap minimum (black rectangles) shifts toward high energy with decreasing T .

Fig. 1(b) are reminiscent of the finite k -mesh used in the DMFT calculations). The spectral weight in the gap region ($|w/T_N| \leq 1$) is mainly of f character, and clearly reduces with decreasing temperature, being qualitatively consistent with the PES spectra so far^{59,62,65–68}.

The results in units of t (Fig. 1) do not match with the experimental spectra. For example, if $t \sim 1$ eV, U becomes 5 eV, T_N becomes 0.2125 eV \sim 2500 K, and the maximum width of the f peak becomes 1 eV. Moreover, the total energy resolution (ΔE) of the experimental setup should be considered in the DMFT spectra to fairly compare each other, which is not feasible with this energy scale. Hence, it is difficult to compare with experimental spectra quantitatively. Interestingly, with the assumption of $t \sim 1$ eV, both T_{coh} and the peak width are about two orders of magnitude higher than the PES results of SmB₆^{62,65}. Hence, a proper scaling factor might exist and provide the connection between theoretical and experimental energy scales. In order to extract T_{coh} in the experiment data ($T_{\text{coh}}^{\text{exp}}$) corresponding to the T_N , we first look carefully at the unique T dependence of n_f (Fig. 1 (a, inset)). Below T_N , n_f and n_d are almost saturated to the maximum and minimum occupations, respectively. Secondly, we recognize that the intensity at E_F is saturated in both f - and d - DOS (green lines) below T_N .

Based on the two signatures around T_N , we search for $T_{\text{coh}}^{\text{exp}}$ in SmB₆ as determined from experiments. According to the saturation point in the T -dependent Sm valence obtained from the XAS result⁶⁴, the $T_{\text{coh}}^{\text{exp}}$ should be around 50 K. Recent $4f$ character-sensitive PES studies show that the gap opening happens below 60 K^{22,62}. Furthermore, various other experiments revealed a similar characteristic temperature of ~ 50 K^{12,13,45,47,51,64,69–82}. Thus, it is reasonable to define a characteristic temperature out of the PES spectra related to the gap formation of the HF insulator, and connect the theoretical energy scale to the experimental energy and temperature as follows: $w/T_N = E/(k_B T_{\text{coh}}^{\text{exp}})$, and $T/T_N = T^{\text{exp}}/T_{\text{coh}}^{\text{exp}}$ where k_B is the Boltzmann constant. The peak broadening due to the experimental resolution can be also implemented in the theoretical spectra. Thus, the theoretical DOS are broadened in energy w by $T_N \cdot (7 \text{ meV})/(k_B \cdot 50 \text{ K})$.

Universal gap evolution for U/t 5, 6, 7, and 8. In order to demonstrate the universal property of the model applying the T_N -scaling, total DOS, which is the sum of f - and d - DOS, near the gap region are shown for various $U/t = 5, 6, 7$ and 8, in Fig. 2. Estimated T_N/t , values for $U/t = 5, 6, 7$ and 8 are 0.2125, 0.155, 0.0795, and 0.0263, respectively²⁵. With increasing U/t from 5 to 8, T_N decreases by an order of magnitude. Note that after the scaling with the respective T_N , the comparison of the gap openings becomes possible for various U/t . In all spectra, the f peak appears in the range of $-5 \leq w/T_N \leq -3$, and the spectral weight of the gap region decreases with lowering temperature. The gap opening in both mixed valence and local moment regimes is similar to each other. This is the unique characteristics of the HF insulator, showing the gap evolution is universal, *i.e.* mostly independent from the actual set of model parameters. The insets of Fig. 2 illustrate the T dependence of n_f and n_d for various U/t values. Normalizing T by T_N leads to the universal change in the occupation numbers. Below T_N , the occupation numbers saturate to a constant value in all cases. The difference in the high and low T values of n_f and n_d decreases when U/t increases. It is recognizable till $U/t = 7$, where the n_f is slightly larger than 1.1.

Four main characteristics are found in the DMFT spectra as a function of U/t , which become obvious after the scaling and taking care of the resolution. First, a systematic energy shift in the gap minimum apparently appears in the mixed valence regime, *i.e.* $U/t = 5$. Second, at higher U/t , the gap deepens more rapidly with respect to the scaled temperature. Third, at the converted temperature of $T \sim 2T_N$ (red lines), the gap minimum positions at slightly different energies for different U/t . The gap minimum appears below E_F at $U/t = 5$, but it appears at higher energy with increasing U/t . Fourth, the f peak intensity at high temperatures is obviously higher in the mixed valence regime because of the presence of the atomic multiplet ${}^6H_{5/2}$ state. Thus, although the lattice coherence has not been developed, it is still possible to observe the peak structure near E_F ^{35,83}.

Mixed valence: PES vs. DMFT for $U/t = 5$. Figure 3(a) shows the angle-integrated photoemission spectra of SmB₆ divided by the Fermi-Dirac distribution (FDD)⁶² on the reduced energy scale of $T_{\text{coh}}^{\text{exp}}$. The peak at $(E - E_F)/(k_B T_{\text{coh}}^{\text{exp}}) = -5$ is the $4f$ multiplet excitation (${}^6H_{5/2}$) with lowest binding energy. The gap in the PES data is getting deeper with decreasing T , comparable to the behavior observed in the theoretical DOS (as shown in the previous figures). We compare now the experimental and the theoretical spectra in more detail using their functional relation to the scaling. If SmB₆ has the scaling property, the energy and T in the PES spectra can be rescaled to link with the DMFT energy.

To make the calculated DOS directly comparable to the experimental spectrum, we treated the DOS by an established numerical procedure already successfully applied to metallic heavy fermion systems⁸⁴. The total DOS was multiplied by the FDD, and convoluted by a Gaussian function regarding the total resolution. Lastly, the resulting spectrum was normalized to the FDD as shown in Fig. 3(b) in order to get comparable spectra in Fig. 3(a).

As a result, the scaled theoretical and experiment spectra show a surprisingly good agreement in the T dependence of both the $4f$ peak and the gap opening. As already theoretically suggested^{24,25}, the $4f$ energy positions, the line widths of the peaks, and the size of the gap are on the scale of the respective T_{coh} . In particular, both gap developments near T_{coh} are very similar. The gap minima in both theory and experiment, marked with black rectangles in Fig. 3, shift from below E_F toward high energy with elaborating T . Note that when the accuracy of our DMFT results is tested, we find that the gap minima are among the most reliable features in the spectra.

Discussion

Heavy fermions are a canonical example of a multi-scale problem. The bare scales such as the Coulomb repulsion U and conduction electron band width are of several eV. In contrast, the emergent scales, in particular the coherence scale, are measured in units of meV⁸⁵. A realistic multi-scale calculation is prohibitively difficult since it would have to take into account the details of the orbital structure and interactions. Low energy physics can however show signs of universality in the sense that scaling with the appropriate energy scale allows

comparison between different experimental realizations of the phenomena under consideration and with theory. Our study follows precisely this idea. A good account of the low energy behavior of the photoemission spectra can be obtained by scaling the experimental and theoretical data with the corresponding coherence scale and making sure that the theoretical calculations are well in the mixed valence regime^{21,24}.

Our theoretical model is a PAM on a square lattice^{21,24}, which we solve by means of DMFT that maps the lattice problem onto a single Anderson impurity model (SIAM). The DMFT approximation captures the salient many body physics of the paramagnetic phase of heavy fermions⁸⁶. Due to the locality of the approximation only dynamical fluctuations are relevant for the emergence of the coherence scale⁴¹. In this sense we do not expect the spacial degrees of freedom to play a dominant role in the analysis of the temperature dependence of the low energy DOS. In particular in the SIAM, dimensionality enters only in terms of the bare density of states at the Fermi energy and is one of the parameters that determine the Kondo scale.

In our model study we consider a two fold degenerate f band unlike in refs^{7,8,20}. The detailed band structure and its symmetry aspects are very interesting issues in the rare-earth hexaborides¹⁷, which will help to find alternative topological Kondo insulators. Nevertheless, in our model we treat only the lowest-lying two bands, *i.e.* one f band and one d band, in order to capture the general gap evolution. As shown in Fig. 3, the line broadening due to the limited experimental resolution makes the theoretical f peak width comparable to the experimental one (See also the Sec. II of the Supplementary Information for further discussion). Thus, it again appears that our simple model is able to capture the main low-energy features of the DOS.

Hence, this demonstrates that just the universal scales of model calculations are sufficient to reproduce the general gap opening appearing in the experiment. In order to obtain further agreement, only few parameters should be adjusted to realize, in particular, the T dependence of the gap evolution and the occupation numbers. These two features are the most reliable and sensitive characteristics in our theoretical results, which mainly depend on the configuration of the input parameter set, *i.e.* the distinction between local moment and mixed valence regimes. Among our survey parameters, the mixed valence configuration gives the best agreement. Hence, our investigation demonstrates that the key parameters, namely the *coherence temperature* and the *degree of valence mixing*, suffice to realize the experiments. Our finding actually proves that the gap nature of SmB_6 involves the emergence of the coherent renormalized bands in the framework of the Fermi liquid theory. Therefore, the topological phase of SmB_6 can be classified with the topological indices applicable to non-interacting insulators as presumed in various theoretical studies^{4,10,11}.

Methods

Theoretical studies on the T dependence of the electronic structure of heavy fermion insulators (half-filled cases) in 2D square lattice were carried out based on the DMFT⁸⁷, which maps a 2D model onto an auxiliary impurity problem. The impurity problem is then solved by the numerically exact CT-HYB quantum Monte Carlo algorithm. For the simple model study, we use tight binding bands with the same input parameters as in the ref.²⁴, which are normalized with the conduction hopping parameter t , *e.g.* $5.0 \leq U/t \leq 8.0$, $\varepsilon_f/t = -6.0$, the hybridization $V/t = 0.4$, etc. The high resolution photoelectron spectroscopy (PES) experiments were carried out at the UE112-PGM-1b (“I^{3m}”) beamline of BESSY II using a Scienta R4000 analyzer at $3 \text{ K} \leq T^{\text{exp}} \leq 60 \text{ K}$ ⁶². The excitation photon energy was $h\nu = 70 \text{ eV}$, whose constant energy map at E_F covers $k_z = 6\pi/a$ in normal emission, with the high energy resolution of 7 meV . Detailed experimental conditions can be found in ref.⁶².

References

- König, M. *et al.* Quantum spin hall insulator state in HgTe quantum wells. *Science* **318**, 766–770, <http://www.sciencemag.org/content/318/5851/766>, <https://doi.org/10.1126/science.1148047> PMID: 17885096 (2007).
- Kane, C. L. & Mele, E. J. Z_2 topological order and the quantum spin hall effect. *Phys. Rev. Lett.* **95**, 146802, <https://doi.org/10.1103/PhysRevLett.95.146802> (2005).
- Senthil, T. Symmetry-protected topological phases of quantum matter. *Annual Review of Condensed Matter Physics* **6**, 299–324, <https://doi.org/10.1146/annurev-conmatphys-031214-014740> (2015).
- Dzero, M., Sun, K., Galitski, V. & Coleman, P. Topological kondo insulators. *Phys. Rev. Lett.* **104**, 106408, <https://doi.org/10.1103/PhysRevLett.104.106408> (2010).
- Hohenadler, M. & Assaad, F. F. Correlation effects in two-dimensional topological insulators. *Journal of Physics: Condensed Matter* **25**, 143201, <http://stacks.iop.org/0953-8984/25/i=14/a=143201> (2013).
- Fu, L., Kane, C. L. & Mele, E. J. Topological insulators in three dimensions. *Phys. Rev. Lett.* **98**, 106803, <https://doi.org/10.1103/PhysRevLett.98.106803> (2007).
- Takimoto, T. SmB_6 : a promising candidate for a topological insulator. *Journal of the Physical Society of Japan* **80**, 123710, <https://doi.org/10.1143/JPSJ.80.123710> (2011).
- Kang, C.-J. *et al.* Band symmetries of mixed-valence topological insulator: SmB_6 . *Journal of the Physical Society of Japan* **84**, 024722, <https://doi.org/10.7566/JPSJ.84.024722> (2015).
- Deng, X., Haule, K. & Kotliar, G. Plutonium hexaboride is a correlated topological insulator. *Phys. Rev. Lett.* **111**, 176404, <https://doi.org/10.1103/PhysRevLett.111.176404> (2013).
- Baruselli, P. P. & Vojta, M. Distinct topological crystalline phases in models for the strongly correlated topological insulator smB_6 . *Phys. Rev. Lett.* **115**, 156404, <https://doi.org/10.1103/PhysRevLett.115.156404> (2015).
- Legner, M., Rüegg, A. & Sigrist, M. Surface-state spin textures and mirror chern numbers in topological kondo insulators. *Phys. Rev. Lett.* **115**, 156405, <https://doi.org/10.1103/PhysRevLett.115.156405> (2015).
- Allen, J. W., Batlogg, B. & Wachter, P. Large low-temperature hall effect and resistivity in mixed-valent SmB_6 . *Phys. Rev. B* **20**, 4807–4813, <https://doi.org/10.1103/PhysRevB.20.4807> (1979).
- Wolgast, S. *et al.* Low-temperature surface conduction in the kondo insulator smB_6 . *Phys. Rev. B* **88**, 180405, <https://doi.org/10.1103/PhysRevB.88.180405> (2013).
- Martin, R. M. & Allen, J. W. Theory of mixed valence: Metals or small gap insulators (invited). *Journal of Applied Physics* **50**, 7561–7566, <https://doi.org/10.1063/1.326765> (1979).
- Kasuya, T. Mixed-valence state in SmB_6 . *EPL* **26**, 283, <https://doi.org/10.1209/0295-5075/26/4/008> (1994).
- Riseborough, P. S. Heavy fermion semiconductors. *Advances in Physics* **49**, 257–320, <https://doi.org/10.1080/000187300243345> (2000).

17. Hanzawa, K. Theory of intermediate-valence states in sm compounds. *Journal of the Physical Society of Japan* **67**, 3151–3158, <https://doi.org/10.1143/JPSJ.67.3151> (1998).
18. Tran, M.-T., Takimoto, T. & Kim, K.-S. Phase diagram for a topological kondo insulating system. *Phys. Rev. B* **85**, 125128, <https://doi.org/10.1103/PhysRevB.85.125128> (2012).
19. Lu, F., Zhao, J., Weng, H., Fang, Z. & Dai, X. Correlated topological insulators with mixed valence. *Phys. Rev. Lett.* **110**, 096401, <https://doi.org/10.1103/PhysRevLett.110.096401> (2013).
20. Alexandrov, V., Dzero, M. & Coleman, P. Cubic topological kondo insulators. *Phys. Rev. Lett.* **111**, 226403, <https://doi.org/10.1103/PhysRevLett.111.226403> (2013).
21. Werner, J. & Assaad, F. F. Interaction-driven transition between topological states in a kondo insulator. *Phys. Rev. B* **88**, 035113, <https://doi.org/10.1103/PhysRevB.88.035113> (2013).
22. Denlinger, J. D. *et al.* Temperature dependence of linked gap and surface state evolution in the mixed valent topological insulator SmB_6 . *arXiv:1312.6637 [cond-mat]*, <http://arxiv.org/abs/1312.6637> (2013).
23. Nikolić, P. Two-dimensional heavy fermions on the strongly correlated boundaries of kondo topological insulators. *Phys. Rev. B* **90**, 235107, <https://doi.org/10.1103/PhysRevB.90.235107> (2014).
24. Werner, J. & Assaad, F. F. Dynamically generated edge states in topological kondo insulators. *Phys. Rev. B* **89**, 245119, <https://doi.org/10.1103/PhysRevB.89.245119> (2014).
25. Chen, K.-S., Werner, J. & Assaad, F. Optical conductivity of topological kondo insulating states. *Phys. Rev. B* **90**, 115109, <https://doi.org/10.1103/PhysRevB.90.115109> (2014).
26. Baruselli, P. P. & Vojta, M. Kondo holes in topological kondo insulators: Spectral properties and surface quasiparticle interference. *Phys. Rev. B* **89**, 205105, <https://doi.org/10.1103/PhysRevB.89.205105> (2014).
27. Kim, J. *et al.* Termination-dependent surface in-gap states in a potential mixed-valent topological insulator: smb_6 . *Phys. Rev. B* **90**, 075131, <https://doi.org/10.1103/PhysRevB.90.075131> (2014).
28. Legner, M., Rüegg, A. & Sigrist, M. Topological invariants, surface states, and interaction-driven phase transitions in correlated kondo insulators with cubic symmetry. *Phys. Rev. B* **89**, 085110, <https://doi.org/10.1103/PhysRevB.89.085110> (2014).
29. Alexandrov, V. & Coleman, P. End states in a one-dimensional topological kondo insulator in large- n limit. *Phys. Rev. B* **90**, 115147, <https://doi.org/10.1103/PhysRevB.90.115147> (2014).
30. Roy, B., Sau, J. D., Dzero, M. & Galitski, V. Surface theory of a family of topological kondo insulators. *Phys. Rev. B* **90**, 155314, <https://doi.org/10.1103/PhysRevB.90.155314> (2014).
31. Alexandrov, V., Coleman, P. & Erten, O. Kondo breakdown in topological kondo insulators. *Phys. Rev. Lett.* **114**, 177202, <https://doi.org/10.1103/PhysRevLett.114.177202> (2015).
32. Yu, R., Weng, H., Hu, X., Fang, Z. & Dai, X. Model hamiltonian for topological kondo insulator SmB_6 . *New Journal of Physics* **17**, 023012, <http://stacks.iop.org/1367-2630/17/i=2/a=023012> (2015).
33. Peters, R., Yoshida, T., Sakakibara, H. & Kawakami, N. Coexistence of light and heavy surface states in a topological multiband kondo insulator. *Phys. Rev. B* **93**, 235159, <https://doi.org/10.1103/PhysRevB.93.235159> (2016).
34. Erten, O., Ghaemi, P. & Coleman, P. Kondo breakdown and quantum oscillations in smb_6 . *Phys. Rev. Lett.* **116**, 046403, <https://doi.org/10.1103/PhysRevLett.116.046403> (2016).
35. Chazalviel, J. N., Campagna, M., Wertheim, G. K. & Schmidt, P. H. Study of valence mixing in SmB_6 by x-ray photoelectron spectroscopy. *Phys. Rev. B* **14**, 4586–4592, <https://doi.org/10.1103/PhysRevB.14.4586> (1976).
36. Denlinger, J. *et al.* Advances in photoemission spectroscopy of f-electron materials. *Physica B: Condensed Matter* **281–282**, 716–722, [https://doi.org/10.1016/S0921-4526\(99\)00915-1](https://doi.org/10.1016/S0921-4526(99)00915-1) (2000).
37. Min, C.-H. *et al.* Two-component analysis of the 4f multiplet of samarium hexaboride. *Journal of Electron Spectroscopy and Related Phenomena* **199**, 46–50, <http://www.sciencedirect.com/science/article/pii/S0368204815000158>, <https://doi.org/10.1016/j.elspec.2015.01.003> (2015).
38. Cox, D., Bickers, N. & Wilkins, J. Calculated properties of valence fluctuators. *Journal of Magnetism and Magnetic Materials* **54**, 333–337, <http://www.sciencedirect.com/science/article/pii/0304885386906086>, [https://doi.org/10.1016/0304-8853\(86\)90608-6](https://doi.org/10.1016/0304-8853(86)90608-6) (1986).
39. Bickers, N. E., Cox, D. L. & Wilkins, J. W. Thermodynamic, transport, and excitation properties of ce impurities in a model metal: Kondo resonance and universality in the mixed-valent regime. *Phys. Rev. Lett.* **54**, 230–233, <https://doi.org/10.1103/PhysRevLett.54.230> (1985).
40. Haldane, F. D. M. Scaling theory of the asymmetric anderson model. *Phys. Rev. Lett.* **40**, 416–419, <https://doi.org/10.1103/PhysRevLett.40.416> (1978).
41. Hewson, A. C. *The Kondo Problem to Heavy Fermions*, <https://doi.org/10.1017/CBO9780511470752> (Cambridge University Press, 1993).
42. Kang, C.-J., Choi, H. C., Kim, K. & Min, B. I. Topological properties and the dynamical crossover from mixed-valence to kondo-lattice behavior in the golden phase of sms. *Phys. Rev. Lett.* **114**, 166404, <https://doi.org/10.1103/PhysRevLett.114.166404> (2015).
43. Yoshida, T., Fujimoto, S. & Kawakami, N. Correlation effects on a topological insulator at finite temperatures. *Phys. Rev. B* **85**, 125113, <https://doi.org/10.1103/PhysRevB.85.125113> (2012).
44. Gabáni, S. *et al.* Magnetic properties of SmB_6 and sm1-xLaxB_6 solid solutions. *Czech J Phys* **52**, A225–A228, <https://doi.org/10.1007/s10582-002-0054-8> (2002).
45. Cooley, J. C., Aronson, M. C., Fisk, Z. & Canfield, P. C. SmB_6 : kondo insulator or exotic metal? *Phys. Rev. Lett.* **74**, 1629–1632, <https://doi.org/10.1103/PhysRevLett.74.1629> (1995).
46. Kim, D. J., Xia, J. & Fisk, Z. Topological surface state in the Kondo insulator samarium hexaboride. *Nat Mater* **13**, 466–470, <http://www.nature.com/nmat/journal/v13/n5/full/nmat3913.html>, <https://doi.org/10.1038/nmat3913> (2014).
47. Biswas, P. K. *et al.* Low-temperature magnetic fluctuations in the kondo insulator smb_6 . *Phys. Rev. B* **89**, 161107, <https://doi.org/10.1103/PhysRevB.89.161107> (2014).
48. Kang, B. Y. *et al.* Magnetic and nonmagnetic doping dependence of the conducting surface states in smb_6 . *Phys. Rev. B* **94**, 165102, <https://doi.org/10.1103/PhysRevB.94.165102> (2016).
49. Kasuya, T. *et al.* Mechanisms for anomalous properties in smb_6 . *Journal of Magnetism and Magnetic Materials* **31**, 447–450, <http://www.sciencedirect.com/science/article/pii/0304885383903153>, [https://doi.org/10.1016/0304-8853\(83\)90315-3](https://doi.org/10.1016/0304-8853(83)90315-3) (1983).
50. Gorshunov, B. *et al.* Low-energy electrodynamics of SmB_6 . *Phys. Rev. B* **59**, 1808–1814, <https://doi.org/10.1103/PhysRevB.59.1808> (1999).
51. Sluchanko, N. E. *et al.* Low-temperature transport anisotropy and many-body effects in smb_6 . *Phys. Rev. B* **64**, 153103, <https://doi.org/10.1103/PhysRevB.64.153103> (2001).
52. Flachbart, K. *et al.* Energy gap of intermediate-valent smb_6 studied by point-contact spectroscopy. *Phys. Rev. B* **64**, 085104, <https://doi.org/10.1103/PhysRevB.64.085104> (2001).
53. Fuhrman, W. T. *et al.* Interaction driven subgap spin exciton in the kondo insulator smb_6 . *Phys. Rev. Lett.* **114**, 036401, <https://doi.org/10.1103/PhysRevLett.114.036401> (2015).
54. Kapilevich, G. A. *et al.* Incomplete protection of the surface weyl cones of the kondo insulator smb_6 : Spin exciton scattering. *Phys. Rev. B* **92**, 085133, <https://doi.org/10.1103/PhysRevB.92.085133> (2015).
55. Tan, B. S. *et al.* Unconventional fermi surface in an insulating state. *Science* **349**, 287–290, <http://science.sciencemag.org/content/349/6245/287>, <https://doi.org/10.1126/science.aaa7974> (2015).

56. Park, W. K. *et al.* Topological surface states interacting with bulk excitations in the kondo insulator SmB_6 revealed via planar tunneling spectroscopy. *Proceedings of the National Academy of Sciences* **113**, 6599–6604, <http://www.pnas.org/content/113/24/6599.abstract>, <https://doi.org/10.1073/pnas.1606042113> (2016).
57. Xu, Y. *et al.* Bulk fermi surface of charge-neutral excitations in SmB_6 or not: A heat-transport study. *Phys. Rev. Lett.* **116**, 246403, <https://doi.org/10.1103/PhysRevLett.116.246403> (2016).
58. Xu, N. *et al.* Surface and bulk electronic structure of the strongly correlated system SmB_6 and implications for a topological kondo insulator. *Phys. Rev. B* **88**, 121102, <https://doi.org/10.1103/PhysRevB.88.121102> (2013).
59. Jiang, J. *et al.* Observation of possible topological in-gap surface states in the kondo insulator SmB_6 by photoemission. *Nat Commun* **4**, <http://www.nature.com/ncomms/2013/131218/ncomms4010/full/ncomms4010.html>, <https://doi.org/10.1038/ncomms4010> (2013).
60. Neupane, M. *et al.* Surface electronic structure of the topological kondo-insulator candidate correlated electron system SmB_6 . *Nat Commun* **4**, <http://www.nature.com/ncomms/2013/131218/ncomms3991/full/ncomms3991.html>, <https://doi.org/10.1038/ncomms3991> (2013).
61. Frantzeskakis, E. *et al.* Kondo hybridization and the origin of metallic states at the (001) surface of SmB_6 . *Phys. Rev. X* **3**, 041024, <https://doi.org/10.1103/PhysRevX.3.041024> (2013).
62. Min, C.-H. *et al.* Importance of charge fluctuations for the topological phase in SmB_6 . *Phys. Rev. Lett.* **112**, 226402, <https://doi.org/10.1103/PhysRevLett.112.226402> (2014).
63. Hlawenka, P. *et al.* Samarium hexaboride: A trivial surface conductor. *arXiv:1502.01542 [cond-mat]*, <http://arxiv.org/abs/1502.01542>, ArXiv: 1502.01542 (2015).
64. Mizumaki, M., Tsutsui, S. & Iga, F. Temperature dependence of sm valence in SmB_6 studied by x-ray absorption spectroscopy. *J. Phys.: Conf. Ser.* **176**, 012034, <https://doi.org/10.1088/1742-6596/176/1/012034> (2009).
65. Denlinger, J. D. *et al.* *SmB6 Photoemission: Past and Present*, chap. 3, 017038, <https://doi.org/10.7566/JPSCP.3.017038> (2014).
66. Nozawa, S. *et al.* Ultrahigh-resolution and angle-resolved photoemission study of SmB_6 . *Journal of Physics and Chemistry of Solids* **63**, 1223–1226, <http://www.sciencedirect.com/science/article/pii/S0022369702000203>, [https://doi.org/10.1016/S0022-3697\(02\)00020-3](https://doi.org/10.1016/S0022-3697(02)00020-3) (2002).
67. Souma, S., Kumigashira, H., Ito, T., Takahashi, T. & Kunii, S. Direct observation of pseudogap of SmB_6 using ultrahigh-resolution photoemission spectroscopy. *Physica B: Condensed Matter* **312–313**, 329–330, <http://www.sciencedirect.com/science/article/pii/S0921452601011152>, [https://doi.org/10.1016/S0921-4526\(01\)01115-2](https://doi.org/10.1016/S0921-4526(01)01115-2) (2002).
68. Xu, N. *et al.* Exotic kondo crossover in a wide temperature region in the topological kondo insulator SmB_6 revealed by high-resolution arpes. *Phys. Rev. B* **90**, 085148, <https://doi.org/10.1103/PhysRevB.90.085148> (2014).
69. Menth, A., Buehler, E. & Geballe, T. H. Magnetic and semiconducting properties of SmB_6 . *Phys. Rev. Lett.* **22**, 295–297, <https://doi.org/10.1103/PhysRevLett.22.295> (1969).
70. Sluchanko, N. *et al.* Nature of the low-temperature anomalies in the physical properties of the intermediate-valent compound SmB_6 . *Journal of Experimental and Theoretical Physics* **88**, 533–537, <https://doi.org/10.1134/1.558825> (1999).
71. Sluchanko, N. E. *et al.* Intragap states in SmB_6 . *Phys. Rev. B* **61**, 9906–9909, <https://doi.org/10.1103/PhysRevB.61.9906> (2000).
72. Zhang, X. *et al.* Hybridization, inter-ion correlation, and surface states in the kondo insulator SmB_6 . *Phys. Rev. X* **3**, 011011, <https://doi.org/10.1103/PhysRevX.3.011011> (2013).
73. Rößler, S. *et al.* Hybridization gap and fano resonance in SmB_6 . *Proceedings of the National Academy of Sciences* **111**, 4798–4802, <http://www.pnas.org/content/111/13/4798.abstract>, <https://doi.org/10.1073/pnas.1402643111> (2014).
74. Kasuya, T., Takegahara, K., Fujita, T., Tanaka, T. & Bannai, E. Valence Fluctuating State in SmB_6 . *Le Journal de Physique Colloques* **40**, C5–308–C5–313, <https://doi.org/10.1051/jphyscol:19795107> (1979).
75. Phelan, W. A. *et al.* Correlation between bulk thermodynamic measurements and the low-temperature-resistance plateau in SmB_6 . *Phys. Rev. X* **4**, 031012, <https://doi.org/10.1103/PhysRevX.4.031012> (2014).
76. Ruan, W. *et al.* Emergence of a coherent in-gap state in the SmB_6 kondo insulator revealed by scanning tunneling spectroscopy. *Phys. Rev. Lett.* **112**, 136401, <https://doi.org/10.1103/PhysRevLett.112.136401> (2014).
77. Peña, O., MacLaughlin, D. E., Lysak, M. & Fisk, Z. Nmr and spin/charge fluctuations in intermediate valent SmB_6 . *Journal of Applied Physics* **52**, 2152–2154, <https://doi.org/10.1063/1.328860> (1981).
78. Takigawa, M. *et al.* Nmr study of a valence fluctuating compound SmB_6 . *Journal of the Physical Society of Japan* **50**, 2525–2532, <https://doi.org/10.1143/JPSJ.50.2525> (1981).
79. Nyhus, P., Cooper, S. L., Fisk, Z. & Sarrao, J. Low-energy excitations of the correlation-gap insulator SmB_6 : a light-scattering study. *Phys. Rev. B* **55**, 12488–12496, <https://doi.org/10.1103/PhysRevB.55.12488> (1997).
80. Roman, J. *et al.* Transport and magnetic properties of mixed valent SmB_6 . *Physica B: Physics of Condensed Matter* **230–232**, 715–717 (1997).
81. Caldwell, T. *et al.* High-field suppression of in-gap states in the kondo insulator SmB_6 . *Phys. Rev. B* **75**, 075106, <https://doi.org/10.1103/PhysRevB.75.075106> (2007).
82. Yeo, S., Song, K., Hur, N., Fisk, Z. & Schlottmann, P. Effects of eu doping on SmB_6 single crystals. *Phys. Rev. B* **85**, 115125, <https://doi.org/10.1103/PhysRevB.85.115125> (2012).
83. Yamaguchi, J. *et al.* Different evolution of the intrinsic gap in strongly correlated SmB_6 in contrast to YbB_{12} . *New J. Phys.* **15**, 043042, <https://doi.org/10.1088/1367-2630/15/4/043042> (2013).
84. Ehm, D. *et al.* Quantitative line shape analysis of the kondo resonance of cerium compounds. *Physica B: Condensed Matter* **312–313**, 663–665, <http://www.sciencedirect.com/science/article/pii/S0921452601012170>, [https://doi.org/10.1016/S0921-4526\(01\)01217-0](https://doi.org/10.1016/S0921-4526(01)01217-0) (2002).
85. Coleman, P. *Introduction to many body physics* (Cambridge Univ. Press, Cambridge, 2011).
86. Pruschke, T., Bulla, R. & Jarrell, M. Low-energy scale of the periodic anderson model. *Phys. Rev. B* **61**, 12799–12809, <https://doi.org/10.1103/PhysRevB.61.12799> (2000).
87. Georges, A., Kotliar, G., Krauth, W. & Rozenberg, M. J. Dynamical mean-field theory of strongly correlated fermion systems and the limit of infinite dimensions. *Rev. Mod. Phys.* **68**, 13–125, <https://doi.org/10.1103/RevModPhys.68.13> (1996).

Acknowledgements

We thankfully acknowledge stimulating discussions with H.-D. Kim, and J.D. Denlinger. This research was supported by the DFG (through SFB 1170 “ToCoTronics”, projects A01, C01, C06, and Z03). B.K.C. and B.Y.K. were supported by National Research Foundation of Korea (NRF) grants funded by the Korean government (MSIP; Grants No. 2011-0028736 and Bank for Quantum Electronic Materials-BQEM00001).

Author Contributions

C.-H.M. conceived the project. F.G., K.-C.C., J.W., and F.A. developed the DMFT code and performed calculations. H.B., P.L., C.-H.M. and F.R. performed PES measurements. B.K. and C.K. grew the crystals. All authors analyzed the data and wrote the manuscript.

Additional Information

Supplementary information accompanies this paper at <https://doi.org/10.1038/s41598-017-12080-5>.

Competing Interests: The authors declare that they have no competing interests.

Publisher's note: Springer Nature remains neutral with regard to jurisdictional claims in published maps and institutional affiliations.



Open Access This article is licensed under a Creative Commons Attribution 4.0 International License, which permits use, sharing, adaptation, distribution and reproduction in any medium or format, as long as you give appropriate credit to the original author(s) and the source, provide a link to the Creative Commons license, and indicate if changes were made. The images or other third party material in this article are included in the article's Creative Commons license, unless indicated otherwise in a credit line to the material. If material is not included in the article's Creative Commons license and your intended use is not permitted by statutory regulation or exceeds the permitted use, you will need to obtain permission directly from the copyright holder. To view a copy of this license, visit <http://creativecommons.org/licenses/by/4.0/>.

© The Author(s) 2017